University of California, San Diego UCSD-ENG-106

Confinement and dynamics of laser produced plasma expanding across a transverse magnetic field

**S. S. Harilal, M. S. Tillack, B. O'Shay,
C. V. Bindhu and F. Najmabadi**

October 24, 2003

Fusion Division
Center for Energy Research

University of California, San Diego
La Jolla, CA 92093-0417

Confinement and dynamics of laser produced plasma expanding across a transverse magnetic field

S. S. Harilal, M. S. Tillack, B. O'Shay, C. V. Bindhu, F. Najmabadi

University of California San Diego

Center for Energy Research

9500 Gilman Drive, Mail code 0438

La Jolla, CA 92093-0438

The dynamics and confinement of laser created plumes expanding across a transverse magnetic field have been investigated. 1.06 μm, 8 ns pulses from a Nd:YAG laser were used to create an aluminum plasma which was allowed to expand across a 0.64 T magnetic field. Fast photography, emission spectroscopy and time of flight spectroscopy are used as diagnostic tools. Changes in plume structure and dynamics, enhanced emission and ionization and velocity enhancement are observed in the presence of the magnetic field. Photographic studies show the plume is not fully stopped and diffuses across the field. The temperature of the plume is found to increase due to Joule heating and adiabatic compression. The time of flight studies show that all of the species are slowed down significantly. A multiple peak temporal distribution is observed for neutral species.

Key words: Laser Produced Plasma, Magnetic confinement, Plasma emission

PACS: 52.50.Jm; 52.55.Jd; 52.70.kz

I. Introduction

The use of a magnetic field with a laser created plume is especially intriguing, as the magnetic field can be used to help better control the dynamic properties of these transient and energetic plasmas. The collimation and stability properties of plasma flows across a magnetic field is of particular relevance to the propagation of charged particle beams, bipolar flows associated with young stellar objects, solar wind evolution, astrophysical jets, *etc* [1,2]. In the field of inertial fusion, confinement of expanding target plasma using a magnetic field offers a potential means to slow high-energy particles before they implant in surrounding structures. The presence of a magnetic (B) field during the expansion of a laser produced plasma may initiate several interesting physical phenomena [3-12] which includes conversion of the plasma thermal energy into kinetic energy, plume confinement, ion acceleration, emission enhancement, plasma instabilities etc.

Considerable work has been performed previously on the interaction of an expanding plasma cloud with a magnetic field. It has been postulated [13] that a cloud of laser-produced plasma will be stopped by a magnetic field B in a distance $R \sim B^{-2/3}$. Ripin *et. al.* [3,14] studied sub-Alfǿenic plasma expansion in the limit of large ion Larmor radius and reported that the magnetic confinement radius R_b followed the expected $B^{-2/3}$ dependency within ±20% error at intermediate magnetic field values. Before the plasma reached R_b, the leading edge developed distinct flute structures or spikes that projected out from the main plasma body into the magnetic field. Mostovych *et al.* [15] investigated collimation and instability in laser-produced barium plasma in 0.5-1 T transverse magnetic fields and explained the narrowing of the plasma jet in the plane perpendicular to the B field due to curvature of the polarization fields, and flute-like striations in the plane of the B field due to hybrid-velocity shear instabilities occurring in the

boundary of the jet. Even though the magnetic pressure $P_B=B^2/8\pi$ exceeded both the plasma ram pressure $P_r=nmV^2/2$ and the thermal pressure $P_t=nkT$, the jet's tip velocity was not reduced. Dimonte and Wiley [16] investigated magnetic profile and plasma structure during plasma expansion in a magnetic field and found diamagnetic cavity and plasma radii scale with magnetic confinement radius over a wide range of ion magnetization. They also observed plasma instabilities that evolve from short to long wavelengths and affect the evolution of the magnetic field.

Pisarczyk *et al.* [17] reported preliminary results of experimental investigations of a laser-created plasma interaction with a strong external magnetic field (~20 T). They observed an elongated and uniform plasma column that was formed on the axis of the magnetic coils, but the exact mechanism behind this process was not well understood. Investigations were made on the possibility of soft-X-ray and X-ray laser in the magnetically confined plasma column and found population inversion [18,19]. Neogi and Thareja [20,21] investigated laser-produced carbon plasma in a non-uniform magnetic field using emission spectroscopy and fast photography. They observed oscillations in the temporal history of the emitting species, which are attributed to edge instability. They also observed oscillations in the plasma parameters. Peyser *et al.* [22] noticed high energy plasma propagating through high magnetic field gives rise to plasma jets arising due to an E×B drift. Their fast photographic studies showed that the magnetic field in the edge region of the bulk plasma gives rise to velocity shear, and the plasma undergoes a dramatic structuring instability. Recently, VanZeeland *et. al.* [7,23] studied the expansion of a laser-produced plasma into an ambient magnetized plasma capable of supporting Alfv̋en waves. They observed the plume traveled across the background magnetic field along with undergoing electric polarization and generating current structures in the background plasma.

Apart from its basic research importance, the effect of magnetic field on the expansion dynamics of laser-produced plumes also has importance in applied research. The effectiveness of debris reduction using magnetically guided pulsed laser deposition has been demonstrated [24,25]. They used a magnetic field to steer the plasma around a curved arc to the deposition substrate and a significant reduction in large particulates were observed. Kokai and co-workers [26] reported enhanced growth of carbon clusters in presence of a magnetic field during laser ablation of graphite plasma. They explained it as the enhancement of ion-neutral reactions due to an increase of ionic species, resulting from collisional ionization of neutral species through a confinement of electrons, leads to the growth of large carbon cluster ions.

In this paper, the emission features and expansion dynamics of laser ablated aluminum plasma expanding across a transverse magnetic field have been investigated. The 1.06 μm pulses from a Q-switched Nd:YAG laser were used for creating the plume in a vacuum chamber. The ambient magnetic field is supplied by an assembly of 2 permanent magnets mounted in a steel core, to create a maximum field of 0.64 T over a volume 5 cm x 2.5 cm x 1.5 cm. The diagnostic tools used are 2 ns-gated photography, time integrated emission spectroscopy, and time of flight (TOF) emission spectroscopy. For the sake of comparison, plume dynamics in the presence and absence of magnetic field are studied. Emission spectroscopic studies showed a relative enhancement of emission from highly charged species and a considerable decline in intensity from singly ionized and neutral species. The electron density and temperature measurements showed an increase at the plume edges. Time of flight (TOF) investigations showed ion acceleration at short distances for multiply charged ions. The ion and neutral species flight range is greatly reduced by the magnetic field lines. The temporal profiles of neutral species are much more affected by the field in comparison with ionic species profiles.

II. Experimental set up

Details of the experimental set up are given in a recent publication [27]. Briefly, 1.06 μm pulses from a Q-switched Nd: YAG laser (8 ns pulse width) was used to create aluminum plasma in a stainless steel vacuum chamber. The chamber was pumped using a high-speed turbo-molecular pump and a base pressure ~10^{-8} Torr was achieved. The aluminum target in the form of a disk was rotated about an axis parallel to the laser beam in order to reduce drilling. The laser beam was attenuated by a combination of wave plate and cube beam splitter and focused onto the target surface at normal incidence using an antireflection-coated plano-convex lens. The beam energy was monitored using an energy meter.

The plume imaging was accomplished using an intensified charged coupled device (ICCD, PI MAX, Model 512 RB) placed orthogonal to the plasma expansion direction. A Nikon lens was used to image the plume region onto the camera to form a 2-dimensional image of the plume intensity. The visible radiation from the plasma was recorded integrally in the wavelength range 350-900 nm. A programmable timing generator was used to control the delay time between the laser pulse and the imaging system with overall temporal resolution of 1 ns.

For spectroscopy studies, an optical system was used to image the plasma plume onto the entrance slit of the monochromator/Spectrograph (Acton Pro, Spectra-Pro 500i), so as to have one-to-one correspondence with the sampled area of the plume and the image. One of the exit ports of the spectrograph was coupled to an intensified CCD camera and the other exit port was coupled to a photomultiplier tube (PMT). By translating the optical system along the direction of target normal, spatial-temporal information of the plume emission could be detected as described previously [27]. For time resolved studies of a particular species in the plume, the specific lines are selected by tuning the grating and imaging onto the slit of the PMT. For recording the

temporal profiles, the output of the PMT was directly coupled to a 1-GHz Digital Phosphor Oscilloscope.

A magnetic trap was fabricated for performing plume expansion studies into a magnetic field. Our modeling results showed that a magnetic circuit closed by magnetic steel could provide a higher magnetic field in the gap as compared with an isolated pair of magnetized plates [28]. The schematic of the magnetic trap used in the experiment is given in fig. 1. Two neodymium magnets (5 cm × 2.5 cm × 1.5 cm) with a maximum field of 1.3 T were used for making the magnetic trap. Magnetic flux measurements were made using a three-channel Advanced Gauss/Tesla-Meter (F.W. Bell, Model 7030). The separation between the magnets was kept at 1.5 cm. Fig. 2 shows the measured distribution of the transverse component of the magnetic field as a function of distance along the plume expansion axis at different positions along with width of the magnets. The maximum magnetic field is 0.64 T and is almost uniform along the direction of the plume expansion. But the field strength is non-uniform in the radial direction (perpendicular to plume expansion direction). The target is placed at a distance 1 cm from the pole edges. This leads to uniform magnetic field along the plume expansion direction.

III. Results and discussion

Ablation of aluminum in vacuum creates an intensely luminous plume that expands normal to the target surface. The base operating pressure and the laser irradiance were kept at ~1×10^{-5} Torr and 4 GW cm^{-2} respectively for all the measurements. When we insert a magnetic field the plume expansion dynamics changed significantly. The main findings are:

(i) The plume expands freely in vacuum without a magnetic field. As it expands across a magnetic field, the plume front decelerates in a direction normal to the target surface. The plume doesn't stop completely; instead, it diffuses slowly across the magnetic

field. The plume tries to expand along the direction of the magnetic field lines indicating lateral expansion.

(ii) The plume lifetime is found to increase in the presence of the magnetic field.

(iii) In the presence of the field, enhanced emission from Al^{++} ions is observed relative to the field free case, while the emission from singly charged (Al^{+}) and neutral species (Al) considerably reduced. In the field free case, the emission intensity of all lines drop off with distance and persist until 20-25 mm from the target surface. In the presence of the field, the emission from all species declines very rapidly with distance and ceased completely around 8-10 mm from the target surface.

(iv) The plume temperature is found to be noticeably influenced by the field. The plume becomes hotter with distance from the target surface. The density of the plume is nearly doubled at earlier times in the presence of the field.

(v) A velocity enhancement is observed for multiply charged ion species at shorter distances. TOF profiles of neutral and singly ionized species showed deceleration while expanding across the magnetic field. In the presence of the magnetic field, the temporal profiles of ionic species are broadened in time, while the single peak distribution of the excited neutral Al species is transformed into a multiple peak distribution.

Details of the results are given in the following sections

A. Plume imaging

Fast photography using an ICCD provides two-dimensional snap shots of the three-dimensional plume propagation. This technique provides details of the expansion dynamics of the plasma

[29,30]. Plasma emission begins on the target surface soon after the laser photons reach the surface. Images of the time evolution of the expanding aluminum plasma with and without a magnetic trap, taken after the onset of the plasma formation, are given in fig. 3. The duration of the intensification (exposure time) is 2 ns and each image is obtained from a single laser pulse. Timing jitter is less than 1 ns. All of the images given in the figures are normalized to the maximum intensity in that image. It should be remembered that each image represents the spectrally integrated plume in the region 350-900 nm that is due to emission from the excited states of various species. They are not necessary representative of the total flux because a part of the plume is nonluminous.

It is well known that the plume expands freely at vacuum conditions [27]. Plasma expansion into a vacuum environment is simply adiabatic and can be fully predicted by theoretical models and numerical gas dynamic simulations [31]. The plume changed significantly when ablation took place in the magnetic trap. When the plume expands across a magnetic field a relatively sharp boundary is formed between the field and the plasma. Fig. 4 gives the position-time (R-t) plot obtained from the imaging data. The symbols in the figure represent experimental data points and the curves represent the best fit. Without magnetic filed the plume front behaves linearly with time (the straight-line fit in the graph corresponds to $R \propto t$). This indicates free expansion of the plume into vacuum. The expansion velocities of the plasmas are measured from the slopes of the displacement–time graph. The estimated expansion velocity of the plume in the field free case is 6.6×10^6 cm/s. When we introduce the magnetic trap, the plume expansion velocity is dropped to 4×10^6 cm/s in the initial times and propagate much slower at times > 150 ns. It is also interesting to note that the plume is not fully stopped by the magnetic field. It indicates that the plume front penetrates into the magnetic field and propagates slowly. While

expanding in the direction perpendicular to the magnetic field, the plume simultaneously expands along the magnetic field. The radial expansion velocity is lower compared to the peak expansion velocity along the axial direction (normal to the target surface).

The magnitude and the effect of the plasma-magnetic field interaction mainly depends on the properties of the outer layer of the plume which effectively shields the interior of the plasma from the magnetic field [6]. As the plume expands freely across a magnetic field, with time the plasma pressure decreases and hence the resistance offered by magnetic field increases. When the pressure of the plasma is greater than the magnetic pressure, the plasma is expected to penetrate through the region occupied by the magnetic field. The plasma confinement and stagnation take place when the magnetic and plasma pressure balance. The confinement should increase the collision frequency of the charged species both by confining them to a smaller volume and by increasing their oscillation frequency. Hence the constraint of the cross-field expansion by the magnetic field results in thermalization and a high pressure in the confined plasma[8]. But particles with velocity components directed only along the magnetic axis will be unaffected by the magnetic field. There is nothing to prevent the plasma from flowing freely along the field lines. So continued expansion in response to this pressure can occur only in the direction of the magnetic field axis. In the present studies, the lateral expansion of the plume (that is in the direction of the field lines) is more pronounced at later times compared to expansion normal to the target surface (see fig. 3).

Plasma collimation or focusing was observed by Mostovych et. al. [15], when the plume expanded across a magnetic field. Compared to the present work, the magnetic pressure in ref.[15] is much larger than thermal as well as ram pressure, ie. low β, and hence diamagnetic currents are weak. They described narrowing of the plume across the field is due to curvature of

the polarization fields. According to them, the plume becomes polarized due to Lorentz force that in turn creates an electric field which causes the entire plasma to Ex B drift across the background magnetic field as described by Borovsky [32]. Payser et. al. [22] also reported similar collimation of the plume with high plasma β. Recent experiments by VanZeeland et. al [23] also is in agreement with the model described in [15]. In their work, the laser created plume is allowed to expand across a magnetized background plasma which undergoes electric polarization and generating current structures in the background plasma. The background plasma in turn generating a variety of waves, mainly shear Alfŵen wave radiation.

B. Emission Spectroscopy

A detailed spectroscopic study is useful for characterizing the plume. Our spectroscopic studies show that most of the species emitted by laser produced aluminum plasma in the present experimental conditions are excited neutral Al species along with Al^{+} and Al^{++}. In the absence of the magnetic field, spectral intensity falls gradually with distance and spectral details persist even at 20 mm from the target. With B field, the spectral line emission showed somewhat different tendency. Figs. 5a and 5b show the time integrated emission spectra recorded at 3 mm and 6 mm with and without the magnetic field. The main lines evident in these spectra are Al^{+} (358.7 nm), Al^{++} (360.16 nm, 361.2 nm), Al (394.4 nm and 396.1 nm). Comparison between the charts indicates that a significant emission enhancement is observed for Al^{++} species while emission intensity of Al^{+} and Al are considerably reduced when the plume expands across magnetic field, all other conditions being unchanged. In the presence of the field, the intensities of all lines regardless of their charge state drops much rapidly with space, especially after 5 mm from the target surface, and become difficult or impossible to detect beyond about 10 mm.

Rai et . al[33] observed enhanced emission from the plume in the presence of magnetic field and ascribed it to an increase in the rate of radiative recombination in the plasma. But we rule out this mechanism as no line emission of Al^{+++} is detected even very close to the target surface. Moreover, we haven't observed intensity increase for Al^{+} or neutral Al species. Another possibility is the formation of these highly charged species through electron-impact excitation in the plume or a rise in the mean electron energy in the plasma. The excitation rate for electron impact is given by,

$$R = n_e N(\sigma v_e) \qquad (1)$$

where n_e is the electron density; N is the ion or neutral density; (σv_e) is the product of ionization cross-section for the electron impact and velocity of the electrons, which is a function of temperature [34]. Enhanced emission from the higher charged species indicates higher excitation rate for electron impact as a result of increased (σv_e). This indicates increased electron energy or electron temperature in the presence of the field. The rapid decline in the intensity and deceleration of singly charged ions and neutrals may be caused by energy transfer in the plasma that involves energy exchange via charge exchange and impact ionization.

For the study of plasma-magnetic field interaction a detailed knowledge of the plume parameters are necessary. In order to determine the density and temperature of the plasma spectroscopic methods are used [35]. The plasma electron temperature (T_e) was measured at various distances using relative intensities of the species having the same ionization. Boltzmann plots of Al^{+} lines at 281.6 nm, 466.3 nm, 559.2 nm and 624 nm were made in order to calculate electron temperature at different distances normal to the target surface. The self-absorption of the Al^{+} transitions selected for temperature measurements were reported to be negligible [36]. Transition probabilities of these lines were taken from the literature [37]. The plasma electron

density was measured using Stark broadened profiles of Al^+ lines. Line shape analyses were repeated at different distances from the target surface, which provides a direct indication of the spatial evolution of electron density, giving an insight into the basic ionization processes taking place in pulsed laser ablation [38]. For the electron density measurements the broadening of the 281.6 nm Al^+ line is selected. The impact parameter is obtained from Griem [37].

The spatial dependence of electron temperature and density of the plasma is given in figs. 6 and 7. For these studies time integrated intensities were used. The value of density and temperature presented at different distances from the target should be regarded as indicative of the average conditions occurring in the plume, rather than defining the conditions at a particular stage of its evolution. In the absence of the magnetic field the temperature and density show a decreasing behavior with distance. With increasing separation from the target surface, the electron temperature falls from 2.75 eV at 1 mm to 1 eV at 12 mm while electron density decreases from 9.7×10^{17} cm^{-3} at 1 mm to 5×10^{17} cm^{-3} at 12 mm. The variation of density as a function of distance follows approximately a 1/z law at short distances, indicating that the initial expansion is one-dimensional which is in good agreement with an adiabatic expansion model [31].

Fig. 7 shows the electron density values are not much affected by the presence of the magnetic field. The plume temperature is also not much affected by the field at short distances. The temperature drops rapidly with increasing distance from the target surface. The mechanism by which the plasma cooled at short distances appeared to be adiabatic expansion. But the presence of the field slowed the cooling process and the temperature is found to increase at distances greater than 4 mm. Compared to the field free case, the increase in temperature at greater distances indicates that gas dynamic effects are less important and the magnetic field has

a strong effect on the heating and confinement of the plasma. Please also note that the values given in fig. 6 are the time averaged values of electron temperature. So the instantaneous temperature at earlier time is expected to be much higher.

The increase in electron temperature relative to the field free case is caused by two effects; (i) Resistive Ohmic/Joule heating and (ii) adiabatic compression of the plasma by the magnetic field. Joule heating can be understood by considering a magnetohydrodynamic (MHD) model to describe the expansion of the ionized plume in a magnetic field. According to this model the generalized form of Ohm's law is given by [39]

$$E + V \times B = J/\sigma_0 + (J \times B)/n_e e \qquad (2)$$

where, E and B are the electric and magnetic fields; V, the mass flow velocity; J, the electron conduction current; σ_0, the conductivity. As the plume expands across the magnetic field, heating can occur due to the energy gained by the electrons from the plume kinetic energy (work is done against the $J \times B$ term that acts to decelerate the flow). The $J \times B$ force acts to push the plasma until the magnetic pressure is balanced by the plasma pressure. This will lead to Joule heating of the electrons so that electrons can continue to excite higher charge states. So the magnetic field promotes electron collisional ionization, which would result in the enhancement of the ion fraction.

According to theoretical calculations, as the plasma expands across a magnetic field an increase in density and temperature at the edges of the plasma is expected [40]. But our time integrated density measurements showed no increase in density in the presence of the magnetic field. Since the plasma edges are expected to be much denser compared to the free expanding interior, there should be a back flow toward the interior which may lead to homogenization of the density profile [40].

Since time averaged measurements do not yield density information at earlier times, we performed time resolved electron density measurements by setting the gate width of the intensifier at 10 ns. Fig. 8 gives the time evolution of electron density recorded at 1 mm from the target surface in the presence and absence of magnetic field. At shorter times (< 40 ns) the line to continuum ratio is small and the density measurement is very sensitive to errors in setting the true continuum level. For times ≥ 40 ns, the line to continuum ratios is within reasonable limits. In this case, interference with the continuum measurement is not severe and the values of n_e shown in the figure should be reliable. Initially the plasma expands isothermally within the time of the duration of the laser pulse. After the termination of the laser pulse, the plasma expands adiabatically. During this expansion the thermal energy is converted into kinetic energy and the plasma cools down rapidly. It can be seen from the figure that the electron density nearly doubled with the presence of the field at initial times. At 40 ns the measured electron density is 7.2×10^{18} cm^{-3} compared to 3.7×10^{18} cm^{-3} with field free case. So the electron density at the plume front position is higher when the plasma expands across the field and inside the plume its value is more or less the same as the field free case because of the back flow.

In order to stop the plasma propagation across a magnetic field, the magnetic pressure must be equal to the plasma pressure; if the magnetic pressure exceeds the plasma kinetic pressure, the plasma will be compressed by the magnetic field. In the present experiments, as our imaging studies showed the plume is not completely stopped by the magnetic field, but it is significantly slowed down similar to plume expansion across a moderate ambient pressure [41]. It indicates that plasma species diffuse into the magnetic field. In order to get more details about the plasma species kinetic behavior, TOF emission studies were made for different species in the plasma with and without magnetic field and are given in the following section.

C. Time of Flight Studies

Time of Flight (TOF) studies of the plasma give vital information regarding the time taken by a particular state of the constituent to evolve after the plasma is formed [42]. This technique gives details on the velocity of the emitted particles and parameters that are of fundamental importance in establishing the mechanisms responsible for the particle emission [43]. To study the influence of magnetic field on different species in the plasma, TOF profiles are taken at different distances from the target surface in the presence and absence of magnetic field. Time resolved studies were made for Al (396.1 nm, $3s^2\,(^1S)3p - 3s^2\,(^1S)4s$), Al^+ (358.6 nm, $3s3d - 3s4f$) and Al^{++} (360.1 nm, 3d-4p) species in the plume.

Typical TOF profiles are given in figs. 9-11 with and without magnetic field. Without the magnetic field, the emission from all species are found beyond 15 mm from the target surface, while in the presence of the magnetic field the species spatial distribution is limited to 10-12 mm above the target surface. The time delay of the temporal emission peak with respect to the laser pulse is recorded as a function of distance and is used for studying plume expansion. This is useful to determine the escape velocity of different species associated with cross-field plasma decay. The distance-time plots drawn from the TOF profiles are given in figs. 12-14.

In the absence of the magnetic field the plume expands freely as indicated by the straight line fit in the time-distance plots. The expansion velocities of the ionized species are found to increase with degree of ionization, which is consistent with earlier observations [41,43]. The maximum expansion velocities of Al^{++}, Al^+ and Al in the field free case are found to be at $(5.3 \pm 0.2) \times 10^6$ cm/s, $(3.0 \pm 0.1) \times 10^6$ cm/s and $(2.0 \pm 0.12) \times 10^6$ cm/s respectively. It is expected that fast electrons and ions travel at the leading edge of the plume. After the laser action ceases, the charge composition of the plasma is governed by 3-body recombination, which dominates over

radiative and/or dielectronic ones due to the rapid drop in electron temperature as the plasma expands. The ions located at the front of the plasma acquire the largest energy during hydrodynamic acceleration and the interaction time for recombination is very much reduced [27].

When the magnetic field is introduced, several interesting phenomena were observed. (i). Kinetic energies of all species are considerably reduced at distances greater than 4 mm. The velocity distribution of the ionic species is only weakly affected at distances shorter than 4 mm. This suggests that the field had very little effect on the early stages of the development of the plume, because the pressure of the plasma greatly exceeds magnetic pressure. (ii). At short distances, an increase in expansion velocity is observed for Al^{++} species relative to the field free case. An expansion velocity of 6.7×10^6 cm/s is estimated for Al^{++} species at shorter distances indicating ion acceleration. This is likely due to acceleration in the electric field generated by strong electron confinement. (iii). Finally, the neutral Al TOF data showed a double-peak distribution.

It will be convenient to estimate some approximate parameters of the plume. With a magnetic field of 0.64 T, with mass = 27 amu, and with a velocity of 5×10^6 cm/s, the Larmor radius for Al^{++} ions is ~1 cm and its value for Al^{+} ions is 1.3 cm (with a velocity of 3×10^6 cm/s) which is of the order of the characteristic length of the plume. The estimated electron Larmor radius is very small (<1 μm). A rough estimate of Alfŕen velocity (v_a) is made by assuming equal electron and ion temperatures shows $v_a = 5 \times 10^5$ cm/s. Due to the highly transient non-equilibrium nature of the plume, assignment of dimensionless parameters to describe the behavior is somewhat limited in validity. One of the key parameters for expansion into a magnetic field is the plasma beta. The thermal beta (β_t) of the plasma is given by

$$\beta_t = \frac{8\pi n_e k T_e}{B^2} \qquad (3)$$

Time evolution of estimated β_t at 1 mm from the target surface is given in fig. 15. The expansion of the plume will stop when the magnetic pressure is balanced by the plasma pressure or β (plasma pressure/magnetic pressure) = 1. Even though the β_t of the plume is ~ 1 at times >100 ns, our imaging studies showed that the plume is not completely stopped by the magnetic field instead it is slowed down considerably. So the plasma β_t is not the only factor governing the nature of expansion. After the initial conversion of thermal energy into directed energy, the directed β or β_d becomes an important parameter, which is given by,

$$\beta_d = \frac{4\pi n_e m v^2}{B^2} \qquad (4)$$

The estimated values of β_d are also given in fig.15. β_d is seen to vary by over an order of magnitude within the first 20 ns of spectral line emission. In the early phase of the plume expansion, β_d is on the order of a few thousands, indicating that we are in the regime of diamagnetic expansion [22]. The laser produced plasma diamagnetic cavity (magnetic bubble) expands until a total excluded magnetic energy becomes comparable to the total plasma energy. By assuming plume expands spherically and considering it is expanding from a flat surface into 2π steradians the bouncing radius (R_b) or confinement radius can be written as

$$R_b = \left(\frac{3\mu_0 E_l}{\pi B^2} \right)^{1/3} \qquad (5)$$

where E_l is the total plasma energy and B is the applied magnetic field [14,23]. With our experimental parameters, the estimated bounce radius R_b = 0.7 cm. The average deceleration of the plume is given by $g = v^2/2R_b$ and time to stagnation or bubble lifetime is given by $t_b = 2R_b/v$, where v is the velocity of the plume in a direction perpendicular to the target surface. The

estimated values of deceleration and stagnation time by taking plume velocity obtained from the images are $g = 2.5 \times 10^{13}$ cm/s^2 and $t_b = 220$ ns. The values of R_b, g and t_b are in good agreement with R-t plots obtained from the plume images. From the R-t plot it is clear that the plume starts to stagnate after 200 ns, and the effective length of the plume is ~ 0.8 cm and the value of $g = 1 \times 10^{13}$ cm/s^2. Please note that although the plume strongly decelerates as it approaches R_b, it does not stop fully. This may be caused by incomplete exclusion of the field inside the plasma, E × B motion of the plasma in the boundary layer and deviation of the spherical plume expansion approximation [14]. The different parameters estimated for our plasma is given in Table 1.

The directed β is found to vary nearly three orders of magnitude during the plume expansion across the magnetic field. Only after the plume has evolved 280 ns does β_d approach unity, indicating that the displaced magnetic field energy is approximately equal to the kinetic energy of the expanding plasma. So at early times, the charged particles diffuse through the region occupied by the magnetic field and exclude the field. The diffusion coefficient of the charged particles perpendicular to a field is related to field strength through the relation [34]

$$D \propto \frac{1}{B^2 T^{1/2}} \qquad (6)$$

So an increase in temperature will reduce the diffusion across the magnetic field and eventually the plume will slow down considerably. In the later phase of the plume expansion, or non-diamagnetic limit, the plasma cools and the magnetic field is able to diffuse across the boundary relatively fast compared to the time scale of the experiment. The magnetic diffusion time (t_d) is essentially the time required to convert the energy of the magnetic field to Joule heat, which is given by

$$t_d = \frac{4\pi\sigma R_b^2}{c^2} \qquad (7)$$

where σ is the plasma conductivity which can be obtained with Spitzer formula [44]. The estimated magnetic diffusion time with present experimental parameters is 560 ns with Z =1.

The observed slowing down of neutrals and ions in the presence of the field is consistent with an MHD model in which kinetic energy of the expansion is transformed into random electron motion (heating). In the presence of the field, the Al^{++} species move with a reduced velocity of 2.5×10^6 cm/s (at distances > 4 mm) while the velocity of Al^{+} species slows down to 1.4×10^6 cm/s. Compared to the field free case, the expansion velocities of neutral Al species are significantly reduced. The measured velocity for the neutral species is 7.5×10^5 cm/s. A delayed component of the Al species propagates with a velocity 4.5×10^5 cm/s. The velocity measurement indicates that in the presence of the field the deceleration of the species is inversely proportional to its charge state.

An enhancement in expansion velocity is observed at short distances for Al^{++} species relative to the field free case indicating ion acceleration. Such an enhancement in ion energy in the presence of the magnetic field was also observed by previous workers [20,45]. From Maxwell's equations and Ohm's Law, a rapidly changing magnetic field will induce large currents within the plume. These diamagnetic currents exclude the magnetic field from the interior of the plume, and may interact with the steady state magnetic field through the $\mathbf{J}\times\mathbf{B}$ force. This dynamic will simultaneously accelerate and decelerate different regions of the plume depending on the direction of the diamagnetic currents [21]. Moreover, the electric field created by the plasma electrons due to their reflection by the magnetic field can also accelerate the ions. Simulation of laser produced plasma expansion across a magnetic field by Kacenjar *et. al.* [46] also showed that the ions located at the plume front position can be accelerated by the radial

electric field. Our TOF results indeed show that Al^{++} ions have the highest expansion velocity compared to other species in the plasma.

Surprisingly, in the presence of the magnetic filed, the kinetic distributions of the neutral species are most affected compared to ionic species which is difficult to understand. The spectral emission features of neutral Al species showed a twin peak distribution as the plume expands across the field and the decay of the species is considerably increased with the field. Recently, we reported the observation of a multiple peak temporal structure for neutral and singly ionized Al species, as the plume expands into an ambient background gas [27] where gas phase collisions transforms initial temporal distributions into a very different final distribution. In the present experiments gas dynamic effects are negligible as the plume expands into vacuum. Neogi and Thareja [20] also observed multiple peak structure for both neutral and ionic species during the carbon plume expansion into a magnetic field and attributed it to edge instability. In their experiments the plume expanded across a non-uniform magnetic field that may induce more $J \times B$ term. In the present experiments, the magnetic field is almost constant in the direction perpendicular to the target surface. But the field is varying in the radial direction considerably as shown in fig. 2. In principle the neutral species are not going to be affected by the field. But collective effects in the plume as it expands across the field lead to enhanced collision, which may cause slowing of the atomic species. The temporal spreading and decay of the species increase with decreasing charge state and neutral species are much broader compared to other ionic species (see figs. 9-11). The delayed peak in the neutral TOF profile is moving with a velocity 4.5×10^5 cm/s and appears > 700 ns even at shorter distances which is higher than the bubble lifetime. At present the origin of the delayed peak in the TOF profiles of neutral species is

not well understood. One scenario for the evolution of the delayed peak with neutral species is the backflow of the particles towards target after the collapse of the bubble.

IV. Summary

The confinement and dynamics of laser produced plasma expansion across a magnetic field have been investigated using fast photography and optical emission spectroscopy. The presence of a magnetic field during the expansion of the plume leads to plasma deceleration and confinement, enhanced emission intensity from doubly charged ions, ion acceleration, and electron temperature and density increase. A magnetic field of 0.64 T produced plasmas with markedly different geometrical features. Fast photography of the plasma luminosity was very helpful in establishing the qualitative behavior of the plume with field-constrained expansion. It showed the plume is not fully stopped and diffuses across the field. Images also illustrate the plasma expands along the field lines, while its flow is restricted in the transverse direction.

Optical emission spectroscopic studies showed in the presence of the field enhanced emission from multiply charged ions while the emission intensities from singly charged ions and neutral species were considerably reduced. The relative rise in intensity of higher-lying levels is mainly due to a rise in the mean electron energy in the plasma. This is supported by the fact that the electron temperature is also found to increase in the presence of the field. The decrease in intensity of neutral and singly ionized Al species relative to doubly ionized Al species also suggests that the intensity of recombination radiation is strongly reduced by the field. The magnetic confinement and compression of the plasma can transform plasma kinetic energy to thermal energy via increased collision frequencies. Additionally the secondary current induced by the plasma outer boundary will add energy to the plasma via Joule heating. Thus the increase

in temperature with increase in distance as plasma expands across a magnetic field is due to Joule heating and adiabatic compression. The electron density is nearly doubled in the presence of field at early times. A 30% increase in electron temperature is observed near stagnation indicating higher collisionality in the presence of the magnetic field.

The thermal and directed β of the plasma is much greater than 1 at initial stages and the plasma would distort the field by compressing it at the leading edge, leaving a field free region within the plasma. At later times and greater distances, when thermal $\beta \sim 1$, a deceleration of the plasma is seen accompanied by thermalization of the flow energy. Thus the magnetic field acts as a retarding media, slowing the plume development. Similar to the density and velocity, the thermal and directed β will also be a highly dynamic quantity and may vary considerably during plume expansion.

In the presence of magnetic field a velocity enhancement is observed for doubly charged ions caused by radial electric field. All of the plume species are slowed down rapidly especially at distances greater than 4 mm which is consistent with MHD model. The temporal profiles of ionic species are not much affected by the field while the profiles of neutral species are transformed into a multiple peak distribution in the presence of field.

References:

[1] W. Gekelman, M. Van Zeeland, S. Vincena, and P. Pribyl, J. GeoPhysical. Res. - Space Phys. **108** (2003).

[2] H. C. Pant, Physica Scrip. **T50**, 109 (1994).

[3] B. H. Ripin, E. A. McLean, C. K. Manka, C. Pawley, J. A. Stamper, T. A. Peyser, A. N. Mostovych, J. Grun, A. B. Hassam, and J. Huba, Phys. Rev. Lett. **59**, 2299 (1987).

[4] S. Okada, K. Sato, and T. Sekiguchi, Jap. J. Appl. Phys. **20**, 157 (1981).

[5] L. Dirnberger, P. E. Dyer, S. R. Farrar, and P. H. Key, Appl. Phys. A **59**, 311 (1994).

[6] D. W. Koopman, Phys. Fluids **19**, 670 (1976).

[7] M. VanZeeland, W. Gekelman, S. Vincena, and G. Dimonte, Phys. Rev. Lett. **87**, 105001 (2001).

[8] S. Sudo, K. N. Sato, and T. Sekiguchi, J. Phys. D **11**, 389 (1978).

[9] R. G. Tuckfield and F. Schwirzke, Plasma Phys. **11**, 11 (1969).

[10] G. Jellison and C. R. Parsons, Phys. Fluids B **24**, 1787 (1981).

[11] F. S. Tsung, G. J. Morales, and J. N. Leboeuf, Phys. Rev. Lett. **90**, 055004 (2003).

[12] K. J. Mason and J. M. Goldberg, Appl. Spectro. **45**, 370 (1991).

[13] D. K. Bhadra, Physics of Fluids **11**, 234 (1968).

[14] B. H. Ripin, J. D. Huba, E. A. McLean, C. K. Manka, T. Peyser, H. R. Burris, and J. Grun, Phys. Fluids B **5**, 3491 (1993).

[15] A. N. Mostovych, B. H. Ripin, and J. A. Stamper, Phys. Rev. Lett. **62**, 2837 (1989).

[16] G. Dimonte and L. G. Wiley, Phys. Rev. Lett. **67**, 1755 (1991).

[17] T. Pisarczyk, A. Farynski, H. Fiedorowicz, P. Gogolewski, M. Kusnierz, J. Makowski, R. Miklaszewski, M. Mroczkowski, P. Parys, and M. Szczurek, Laser Part. Beams **10**, 767 (1992).

[18] A. Farynski, P. Gogolewski, L. Karpinski, M. Kusnierz, J. Makowski, M. Szczurek, B. A. Bryunetkin, A. J. Faenov, and I. J. Skobelev, Laser Part. Beams **10**, 801 (1992).

[19] S. Suckewer, C. H. Skinner, H. Milchberg, C. Keane, and D. Voorhees, Phys. Rev. Lett. **55**, 1753 (1985).

[20] A. Neogi and R. K. Thareja, J. Appl. Phys. **85**, 1131 (1999).

[21] A. Neogi and R. K. Thareja, Phys. Plasmas **6**, 365 (1999).

[22] T. A. Peyser, C. K. Manka, B. H. Ripin, and G. Ganguli, Phys. Fluids B **4**, 2448 (1992).

[23] M. VanZeeland, W. Gekelman, S. Vincena, and J. Maggs, Phys. Plasmas **10**, 1243 (2003).

[24] R. Jordan, D. Cole, and J. G. Lunney, Appl. Surf. Sci. **110**, 403 (1997).

[25] Y. Y. Tsui, H. Minami, D. Vick, and R. Fedosejevs, J. Vac. Sci. Tech. A **20**, 744 (2002).

[26] F. Kokai, Y. Koga, and R. B. Heimann, Appl. Surf. Sci. **96-98**, 261 (1996).

[27] S. S. Harilal, C. V. Bindhu, M. S. Tillack, F. Najmabadi, and A. C. Gaeris, J. Appl. Phys. **93**, 2380 (2003).

[28] X. Wang, M. S. Tillack, and S. S. Harilal, UCSD-LPLM-02-04 (UC San Diego, Internal Report, 2003).

[29] D. B. Geohegan, in *Pulsed Laser Deposition of Thin Films*, edited by D. B. Chrisey and G. K. Hubler (John Wiley & Sons, Inc., New York, 1994), p. 115.

[30] S. S. Harilal, C. V. Bindhu, V. P. Shevelko, and H. J. Kunze, Laser Part. Beams **19**, 99 (2001).

[31] R. K. Singh and J. Narayan, Phys. Rev. B **41**, 8843 (1990).

[32] J. E. Borovsky, Phys. Fluids B **30**, 2518 (1987).

[33] V. N. Rai, A. K. Rai, F.-Y. Yueh, and P. S. Singh, Appl. Opt. **42**, 2085 (2003).

[34] A. A. Harms, K. F. Schoepf, G. H. Miley, and D. R. Kingdon, *Principles of Fusion Energy* (World Scientific, Singapore, 2000).

[35] H. R. Griem, *Principles of Plasma Spectroscopy* (Cambridge, New York, 1997).

[36] C. Colon, G. Hatem, E. Verdugo, P. Ruiz, and J. Campos, J. Appl. Phys. **73**, 4752 (1993).

[37] H. R. Griem, *Plasma Spectroscopy* (McGraw-Hill, New York, 1964).

[38] S. S. Harilal, C. V. Bindhu, R. C. Issac, V. P. N. Nampoori, and C. P. G. Vallabhan, J. Appl. Phys. **82**, 2140 (1997).

[39] T. J. M. Boyd and J. J. Sanderson, *The Physics of Plasmas* (Cambridege, New York, 2003).

[40] I. B. Bernstein and W. J. Fader, Phys. Fluids **11**, 2209 (1968).

[41] S. S. Harilal, C. V. Bindhu, M. S. Tillack, F. Najmabadi, and A. C. Gaeris, J. Phys. D **35**, 2935 (2002).

[42] S. S. Harilal, Appl. Surf. Sci. **172**, 103 (2001).

[43] S. S. Harilal, R. C. Issac, C. V. Bindhu, V. P. N. Nampoori, and C. P. G. Vallabhan, J. Appl. Phys. **81**, 3637 (1997).

[44] J. D. Huba, *NRL Plasma Formulary* (2002).

[45] H. Schwarz and H. Hora, in *Laser Interaction And Related Plasma Phenomena*, edited by H. Schwarz and H. Hora (Plenum Press, New York, 1971), p. 301.

[46] S. Kacenjar, M. Hausman, M. Keskinen, A. W. Ali, J. Grun, C. K. Manka, E. A. McLean, and B. H. Ripin, Phys. Fluids **29**, 2007 (1986).

Table 1. Different parameters estimated in an Al laser plasma formed from 8-ns, 4 GW/cm^2 pulses in a 0.64 T transverse magnetic field

Al^{++} Larmor radius	1.3 cm
Al^{+} Larmor radius	1 cm
Electron Larmor radius	~1 μm
Plume deceleration (g)	2.5×10^{13} cm/s
Bubble radius (R_b)	0.7 cm
Bubble lifetime (t_b)	220 ns
Confinement time t_s (Al^{++})	254 ns
Confinement time t_s (Al^{+})	460 ns
Magnetic diffusion time ($t_{d)}$	560 ns (Z =1); 330 ns (Z=2)
Plasma thermal β (at 250 ns)	~ 1
Plasma directed β (at 250 ns)	~10

Figure Captions

FIG. 1. Schematic of the magnetic trap used. The separation between the two ceramic magnets was kept at 1.5 cm.

FIG. 2. The magnetic field distribution between the two magnets separated by 1.5 cm measured using a Gauss meter along the plume expansion direction at different axial points. All the measurements were made at a plane 0.75 cm from the magnetic surfaces.

FIG. 3. Plume images recorded using 2 ns gated ICCD camera in the presence and absence of the magnetic field. The times in the figure represent the time after the evolution of the plasma. For better clarity, each image is normalized to its maximum intensity.

FIG. 4. R-t plots obtained from plume images. Without magnetic field, the plume propagates freely. In the presence of field, plume propagation is considerably slowed down and confined in a direction perpendicular to the target surface. Plume expansion in the lateral direction is significantly higher in the presence of the magnetic field.

FIG. 5. The emission spectra recorded at (a) 3 mm and (b) 6 mm from the target in the presence and absence of magnetic field, but otherwise identical conditions.

FIG. 6. The variation of temperature with distance from the target surface in the presence and absence of magnetic field. The solid line represents best-fit curve for without field case.

FIG. 7. Electron density as a function of distance. The solid line represents 1/z curve.

FIG. 8. Time evolution of density measured at 1 mm from the target surface.

FIG. 9. TOF profiles of Al species at 396.1 nm ($3s^2(\,^1S)3p$ - $3s^2(\,^1S)4s$)) recorded at different distances from the target surface. (a) without B and (b) with B.

FIG. 10. TOF profiles of Al^+ species at 358.6 nm,($3s3d$ - $3s4f$) in the absence (a) and presence of B field (b).

FIG. 11. Temporal emission profiles of Al^{++} at 360.1 nm (3p-4d) recorded at different distances from the target surface (a) without B and (b) with B.

FIG. 12. R-t plots for Al species obtained from the TOF distributions. With the presence of the field, two kinetic peaks were observed for Al species. The faster and slower peaks are termed Pk1 and Pk2 respectively.

FIG. 13. R-t plots for Al^+ species in the presence and absence of magnetic field.

FIG. 14. R-t plot obtained from TOF profiles of Al^{++} species with and without magnetic field.

Figure 15. The time evolution of the thermal and directed β estimated at 1 mm from the target surface.

Figure 1.

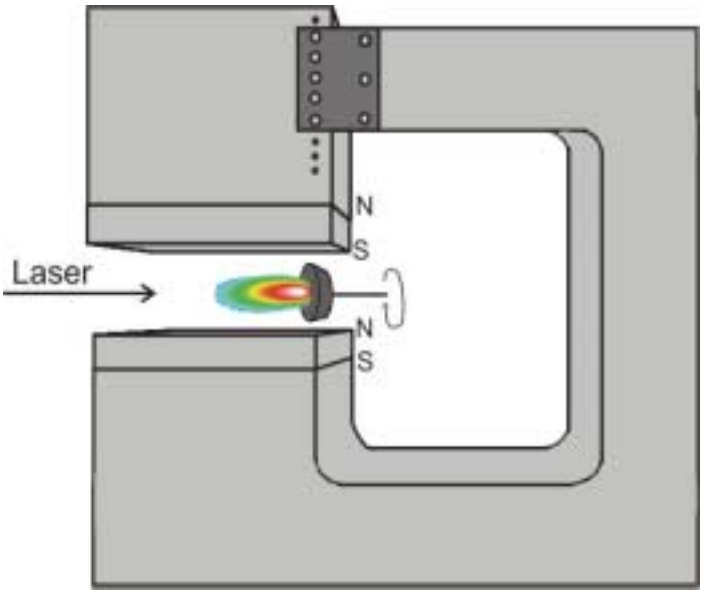

Figure 2.

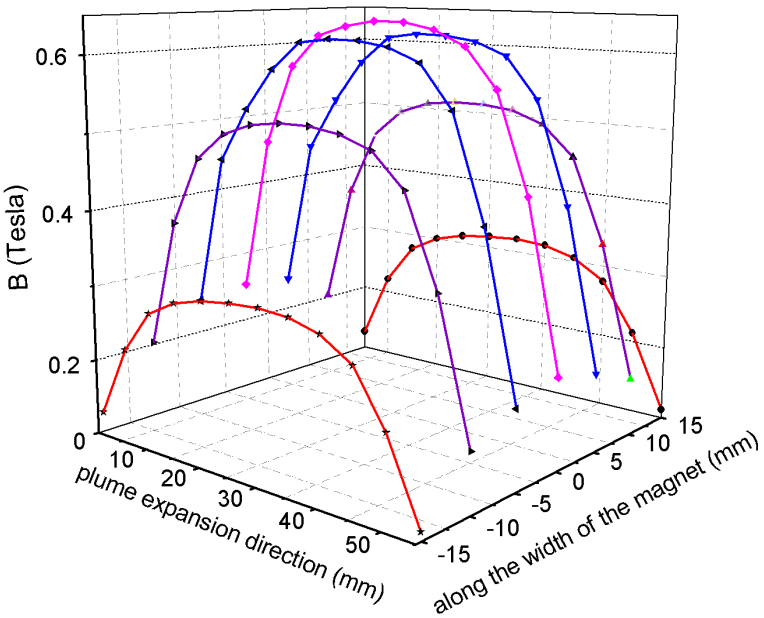

Figure 3.

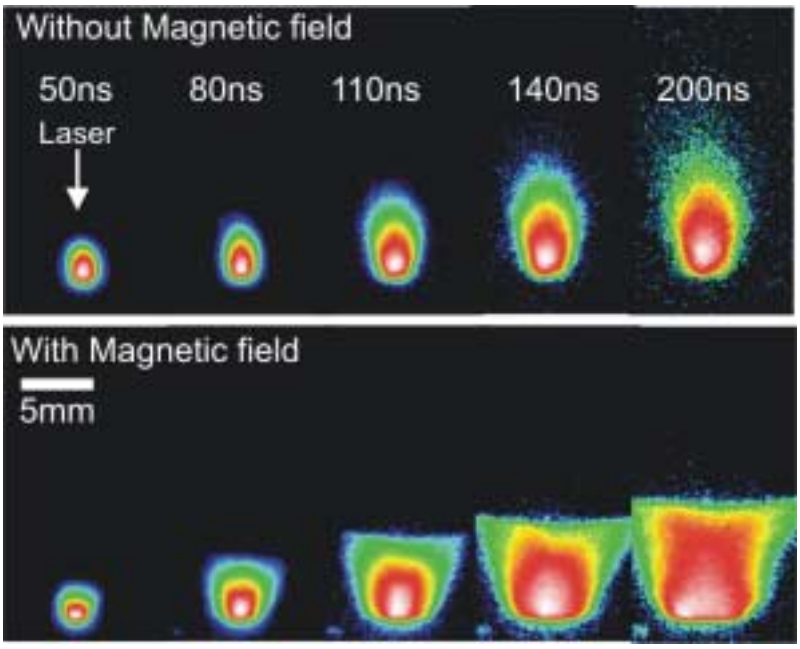

Figure 4

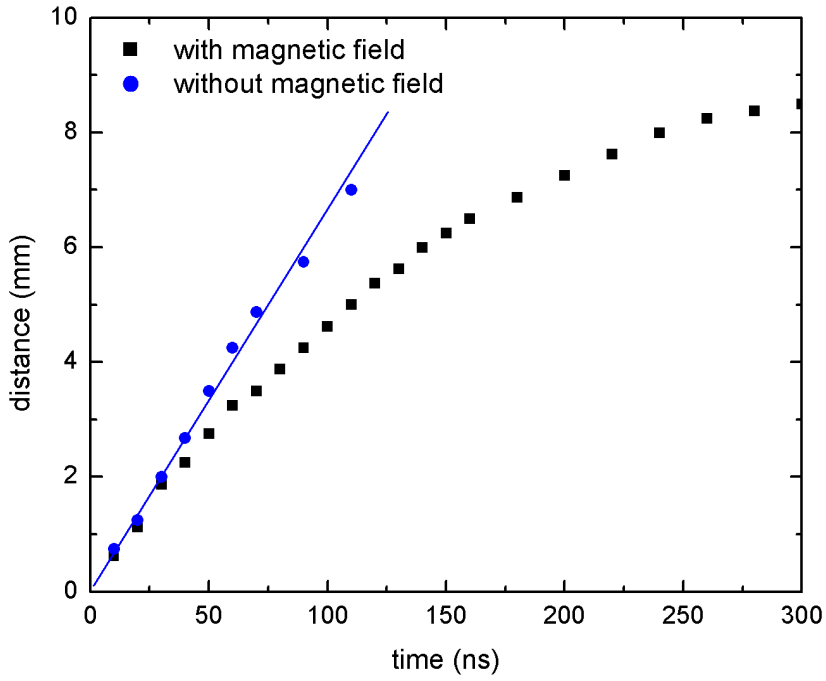

Figure 5 a & b

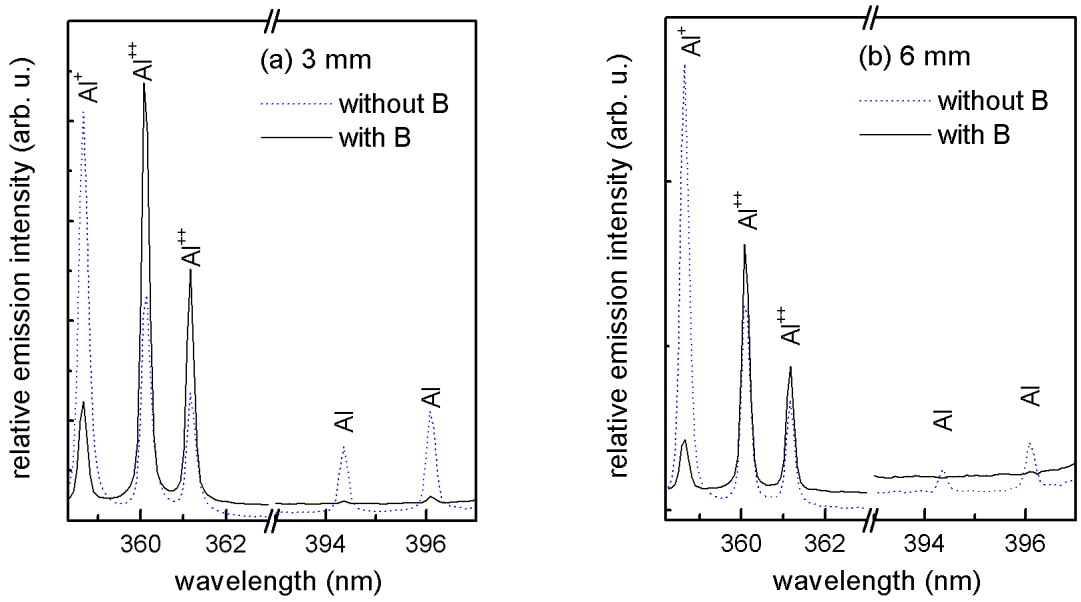

Figure 6.

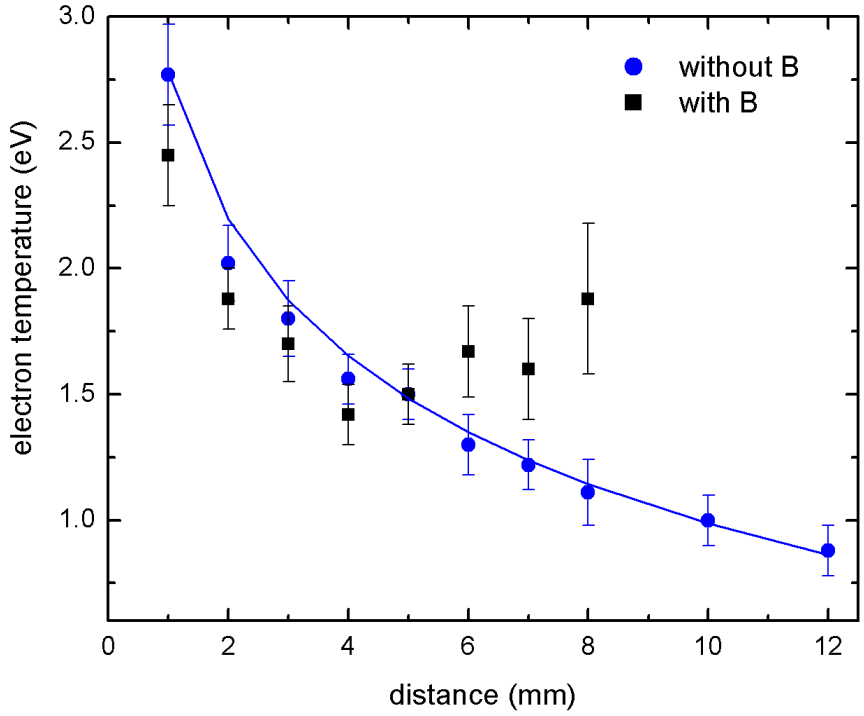

Figure 7.

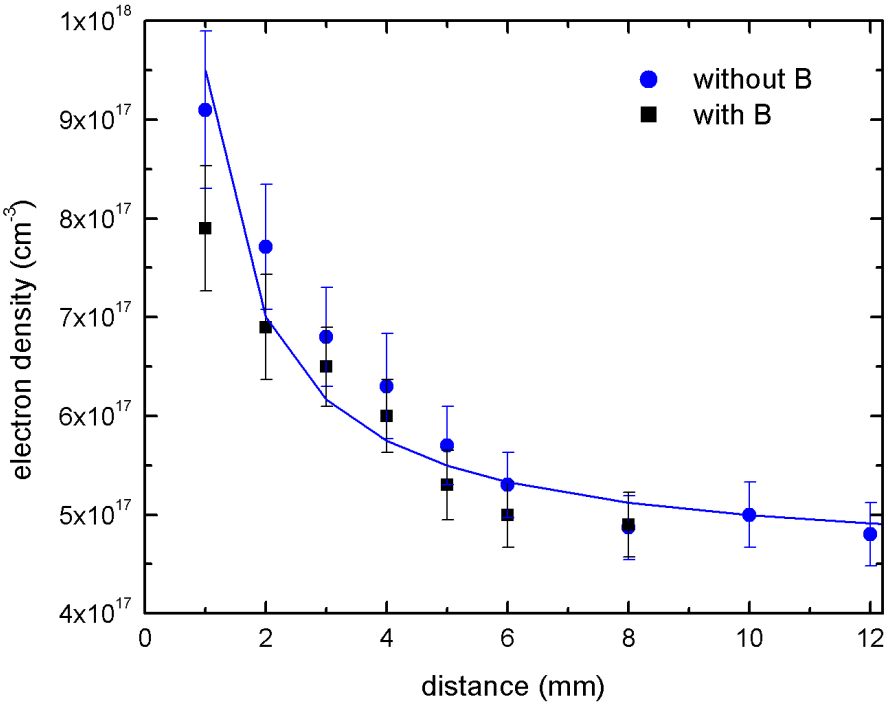

Figure 8.

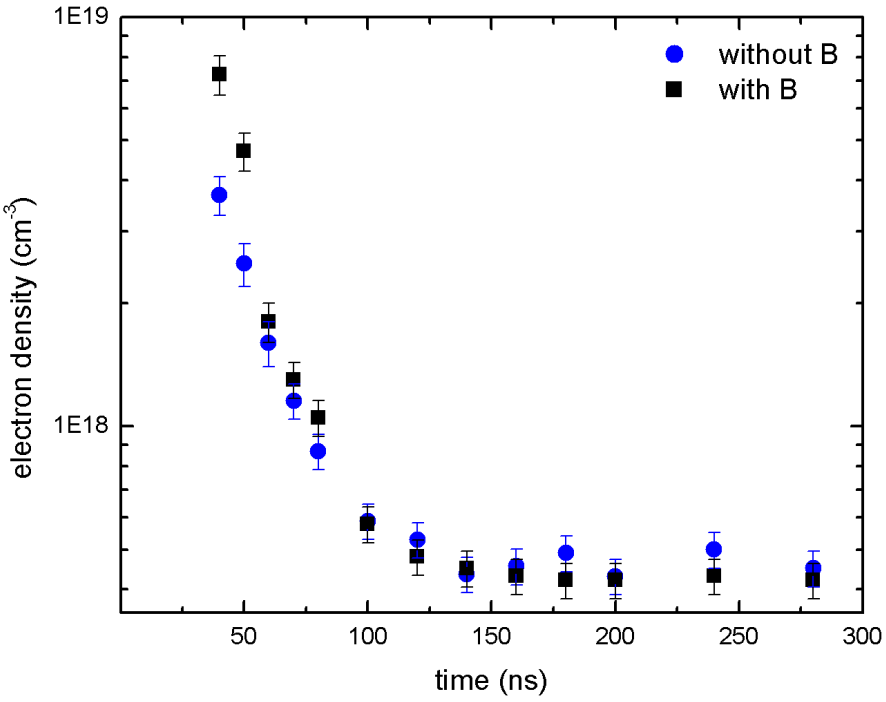

Figure 9a & b.

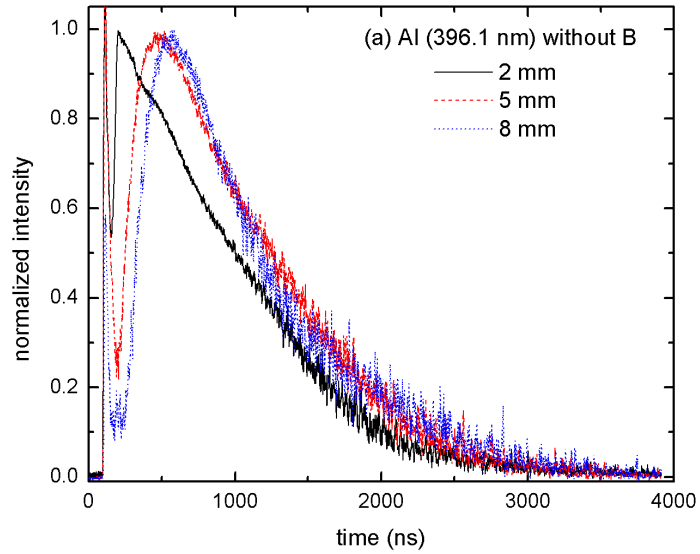
(a) Al (396.1 nm) without B
2 mm
5 mm
8 mm
normalized intensity
time (ns)
0.0
0.2
0.4
0.6
0.8
1.0
0
1000
2000
3000
4000

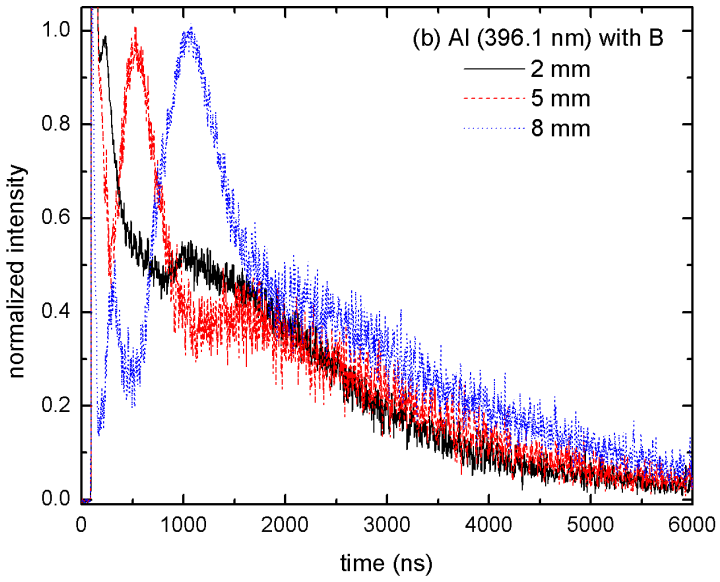
(b) Al (396.1 nm) with B
2 mm
5 mm
8 mm
normalized intensity
time (ns)
0.0
0.2
0.4
0.6
0.8
1.0
0
1000
2000
3000
4000
5000
6000

Figure 10 a & b

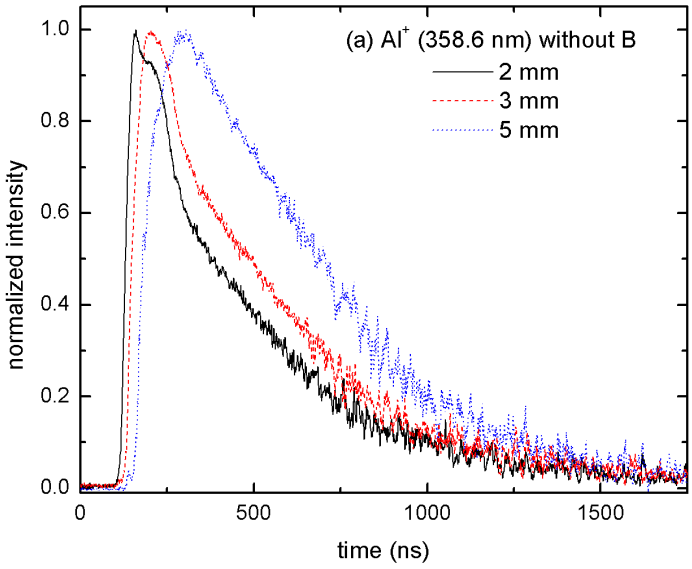
(a) Al+ (358.6 nm) without B
2 mm
3 mm
5 mm
normalized intensity
time (ns)
0.0
0.2
0.4
0.6
0.8
1.0
0
500
1000
1500

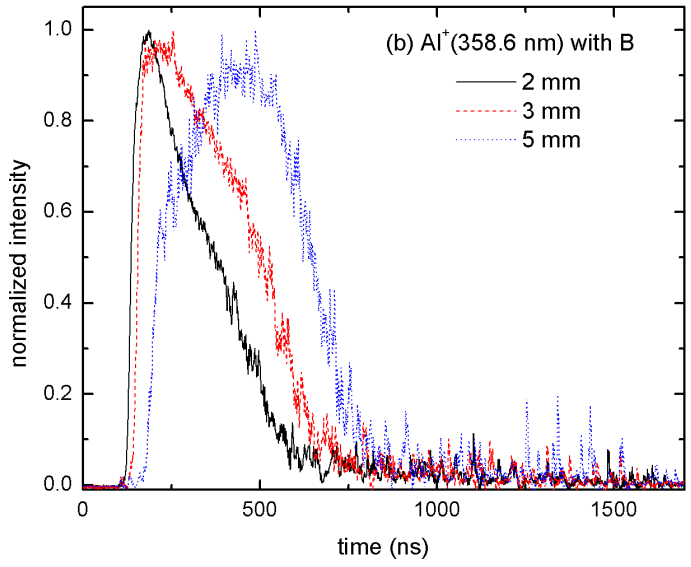
(b) Al+(358.6 nm) with B
2 mm
3 mm
5 mm
normalized intensity
time (ns)
0.0
0.2
0.4
0.6
0.8
1.0
0
500
1000
1500

Figure 11 a & b

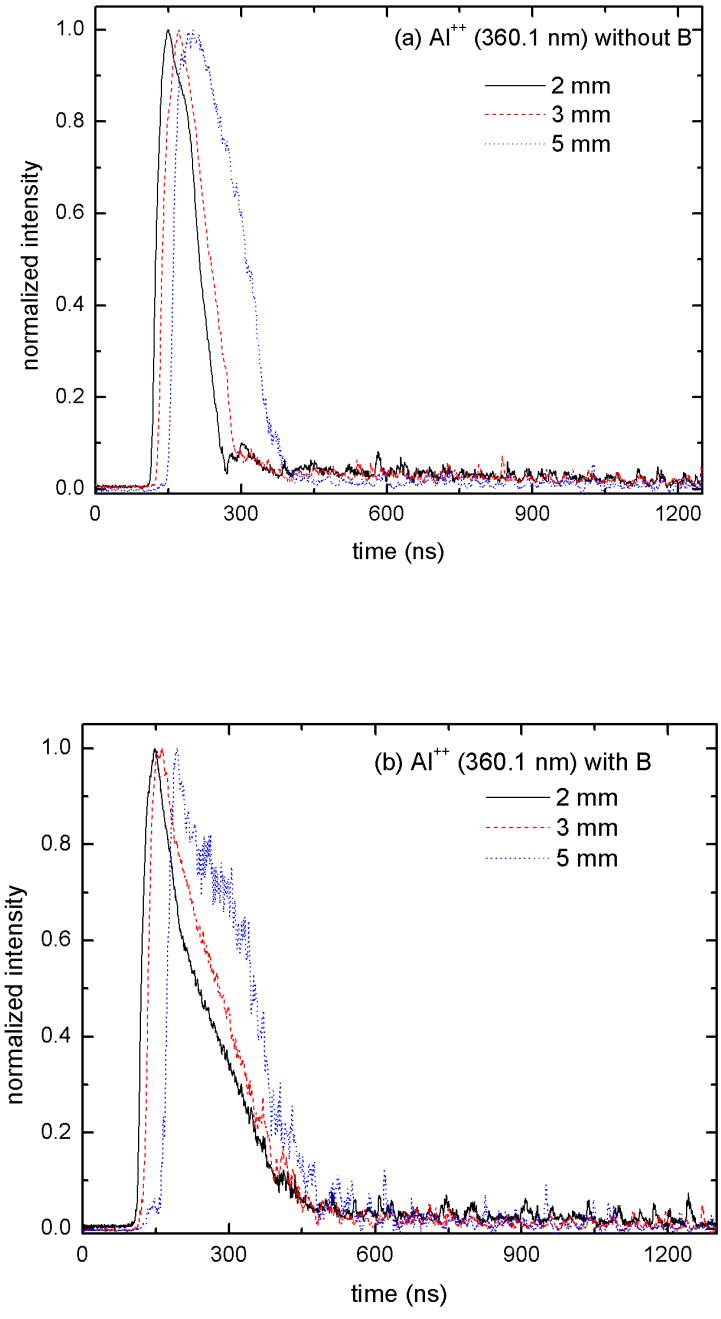
(a) Al++ (360.1 nm) without B
2 mm
3 mm
5 mm
normalized intensity
time (ns)
0.0
0.2
0.4
0.6
0.8
1.0
0
300
600
900
1200
(b) Al++ (360.1 nm) with B
2 mm
3 mm
5 mm
normalized intensity
time (ns)

Figure 12

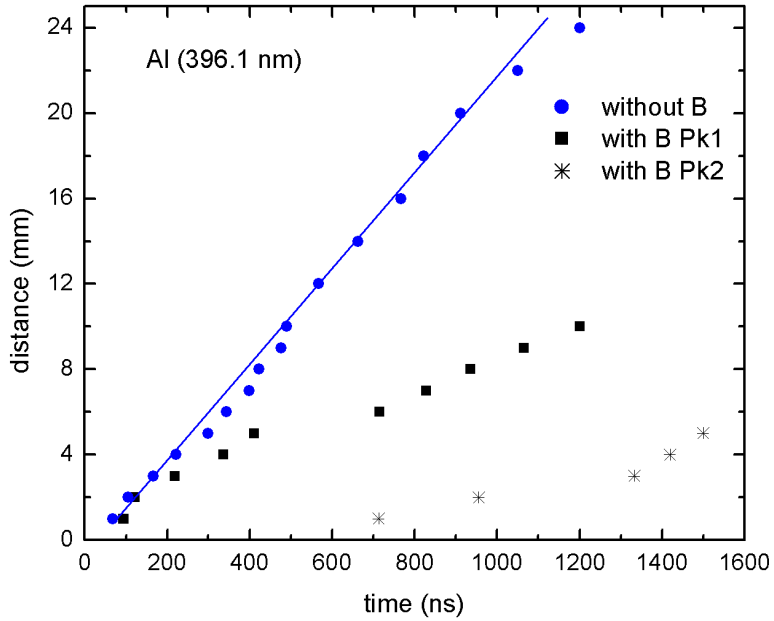

Figure 13.

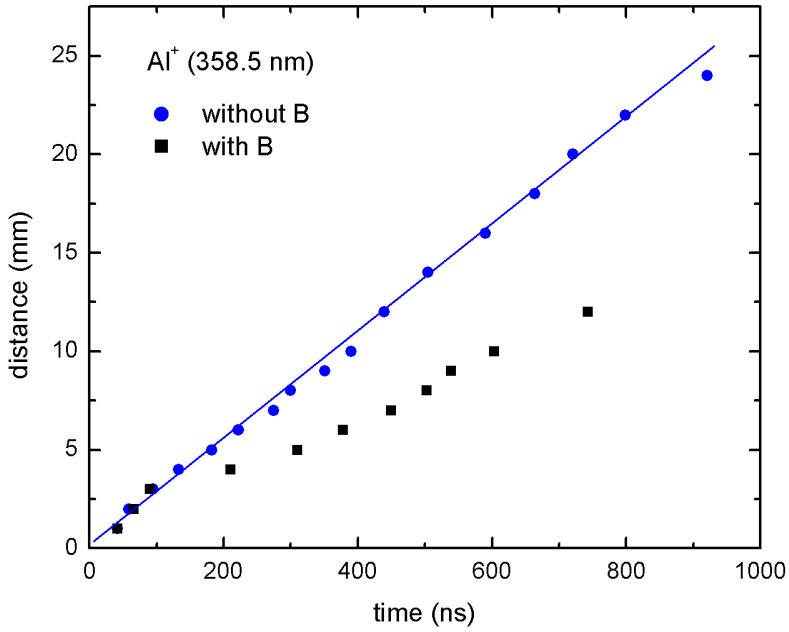

Figure 14.

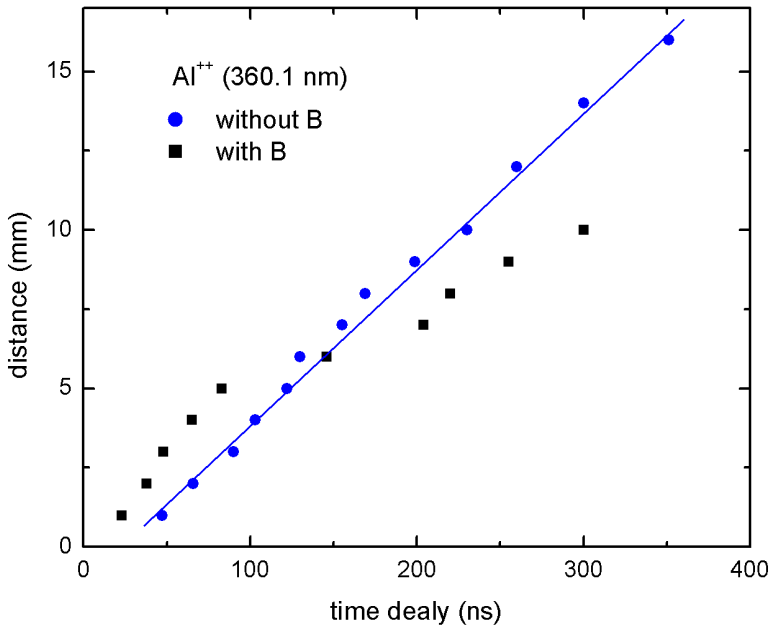

Figure 15